Water vapor, water-ice clouds, and dust in the North Polar Region

L. K. Tamppari, *Jet Propulsion Laboratory/Caltech, Pasadena, CA, USA (leslie.tamppari@jpl.nasa.gov),* **M. D. Smith,** *Goddard Space Flight Center, Greenbelt, MD, USA,* **D. S. Bass, A. S. Hale,** *Jet Propulsion Laboratory/Caltech, Pasadena, CA, USA*

Introduction:

The behavior of water vapor, water-ice and dust in the Martian atmosphere is important for understanding the overall Martian climate system, which is characterized by three main cycles: water, including water-ice, dust, and CO2. Understanding these cycles will lend insight into the behavior of the atmospheric dynamics, the atmosphere's ability to transport dust, water-ice, and vapor to different parts of the planet, and how that ability changes as a function of dust and water-ice loading.

Because the north polar region has the largest detectable source of water present on Mars today (Kieffer 1979; e.g., Boynton et al., 2002), examining water vapor, water-ice clouds and dust in this area is of interest. Furthermore, understanding their behavior may provide insight into the differences in behavior between the polar caps and in the formation of the polar layered deposits.

Water-ice opacities in the north polar region are known to be dominated by polar hood clouds that track the seasonal polar cap in the spring and late summer/early fall (e.g., Leovy et al., 1972; Briggs and Leovy, 1974; James et al., 1994), and to be much smaller in the north polar region than the equatorial region during summer. This can be seen clearly in longitudinally averaged maps such as those provided by Smith (2004, Figure 5). Dust opacities, on the other hand, tend to be higher in the north polar region during spring and summer than in the equatorial regions (e.g., Smith, 2004). This is due to increased frequency of cap-edge dust storms (James and Cantor, 2001).

While observations of water-ice clouds and dust in the Martian atmosphere have been made, previous studies in the north polar region of Mars have either focused on imaging data sets (e.g, Wang and Ingersoll, 2002; James and Cantor, 2001, Cantor et al., 2001) without optical depth estimates or on longitudinally averaged infrared data sets which do provide optical depth estimates (e.g., Smith, 2004; Liu et al., 2003). Additionally, older data set (pre-MGS) either did not have full spectral capability (e.g. Viking Infrared Thermal Mapper [IRTM]) or did not have multi-year coverage (Mariner 9). Water-ice clouds can be detected in the Viking IRTM instrument (Tamppari et al., 2000, 2003), but have not yet been retrieved in the polar regions, although some preliminary latitude-, longitude-, and season-resolved studies using IRTM have been performed (Tamppari and Bass, 2000). Furthermore, dust retrievals have been performed from the IRTM data set (e.g., Martin and Richardson, 1993), but these have been zonally averaged. The MGS spacecraft provides, for the first time, a data set of regular, good resolution, long-term coverage from which to perform such studies.

Smith (2002) examined water vapor in the north polar region, but only examined longitudinally averaged data during the first full MGS year. In his paper, he found that the vapor increase in northern spring, as the seasonal polar cap is subliming and sunlight is hitting the region for the first time that season, appears to be quite rapid in MAWD data, but is more gradual in TES data (Smith, 2002). Farmer et al. (1976) observed a water vapor peak in latitude bands 70-80° at Ls=108. Later MAWD analysis with a more full data set showed a maximum of 100 pr um between 85-90 N at Ls=120 (Jakosky and Farmer, 1982). Sprague et al. (2001) obtained 42 measurements higher than 65 N, spanning 1996-1999. They observed a peak of 76 pr um at about Ls=113, a little early and a little lower latitude than MAWD, though roughly consistent. Smith (2002) shows a maximum of 100 pr m at Ls =115 and 80° N. Sprague et al. (2001) indicate that their ground based measurements show a seasonal maximum much lower than the TES measurements, about 76 pr m at Ls=113 and 75° N (1998-1999 observations). However, their measurements from the previous season, 1996-1997, only show an abundance of ~50 pr m at Ls=114 and 79° N (Sprague et al., 2001).

Water-ice, water vapor, and dust observations are important for the Phoenix Mars Scout mission, scheduled to launch in August 2007 and planning to land in the north polar region between 65-72N. The Phoenix mission is planning to carry two experiments that will observe these quantities in the atmosphere: a solid state imager, developed by the University of Arizona, and an upward-looking lidar, contributed by the Canadian Space Agency. For planning purposes, the amount and behavior of the vapor, ice, and dust is of interest. Furthermore, the Phoenix engineering team is also interested in water-ice and dust opacities. Both water-ice and dust optical depth will affect the amount of sunlight impingent upon the solar panels, thus modifying the amount of solar energy present to power the spacecraft and instruments. Dust in the atmosphere will affect the surface and near-surface atmosphere temperatures, which in turn could affect the amount of heater power needed to keep the spacecraft warm (it

is passively cooled). Finally, the spacecraft entry, descent and landing will be affected by the amount of dust present due to its affect on the atmospheric temperature profile and therefore the density profile that the spacecraft experiences.

Data Sets:

The water vapor and water-ice and dust optical depth mapping done in here utilizes the data from the MGS TES instrument. It is an infrared interferometer/spectrometer operating in the spectral range 6-50μm (Christensen, 1992). In particular, the water-ice clouds are retrieved using the ~12- m (825 cm^{-1}) water-ice absorption feature and the dust is retrieved using the ~9- m (1075 cm^{-1}) (Pearl et al., 2001; Smith, 2004). Water vapor is retrieved using 5 bands spanning 28-42 µm.

The MGS spacecraft is in a sun-synchronous, nearly polar orbit (Christensen, et. al., 2001). The spacecraft orbits Mars 12 times every 1-sol period covering the globe with equally spaced strips once a day. The data are taken around the local time of 1400 hours and 0200 hours. Here, we use the daytime (~1400 hour) data. At this time of day, water-ice clouds formation is likely to be near the minimum since the diurnal temperatures will be near the maximum (e.g., Pathak et al., 2004). As such, water-ice optical depths noted here are likely a lower limit on the amount present over the diurnal cycle.

Mapping of atmospheric quantities:

The atmospheric quantities mapped here, using MGS TES observations, span nearly three Mars spring/summer seasons, from $L_s \approx 104$ in Mars year 24 (1999-2000) to $L_s \approx 180$ in Mars year 26 (2002-2003; Mars years definitions per Clancy et al., 2000). L_s is defined as the areocentric longitude of the sun, with L_s=0 starting at northern spring equinox and stepping through the seasons to L_s=359, just before the subsequent northern spring equinox. The data examined cover 60-90°N latitude during the Mars northern spring and summer times (L_s=0-180). Because of the low surface temperature in these northern latitudes, which decreases the signal to noise, the data examined here are retrieved only over a surface of T>220K.

To produce seasonal maps, we average the optical depths and the vapor in boxes of 2º latitude by 4º longitude by 5º in L_s (Figures 1 and 2 for water-ice and dust, respectively and Figure 3 for water vapor). We chose this combination of parameters to maximize the areal coverage while minimizing the time step from map to map, and to allow averaging of many retrievals together, minimizing the uncertainties in each bin. The mathematical mean is computed for each bin using the total number of points that fell into that lat/lon/Ls bin. The typical number of points in any one bin is 10-20, and so we assume that the uncertainties in each bin are 0.025 or 5% of the optical depth. The color scale for the maps shows absorption-only optical depths for $\tau_{12\mu m}$ (water-ice) on a scale of 0-0.2 and $\tau_{9\mu m}$ (dust) on a scale of 0-0.4. For water vapor, the color scal ranges from 0-100 pr microns. The dynamic range of each of the scale bars was chosen to "stretch" the signal and bring out variations within the maps. In actuality, the largest value in a given map is often larger than the maximum shown and in those cases, is colored to the maximum color on the scale bar. The black area in the maps contains no data. The black area surrounding the north pole is due to surface temperature cutoff of T_s >220K. This area decreases and subsequently increases, following the retreat and growth of the seasonal polar cap.

Maps for all years and seasons will be shown and discussed at the conference.

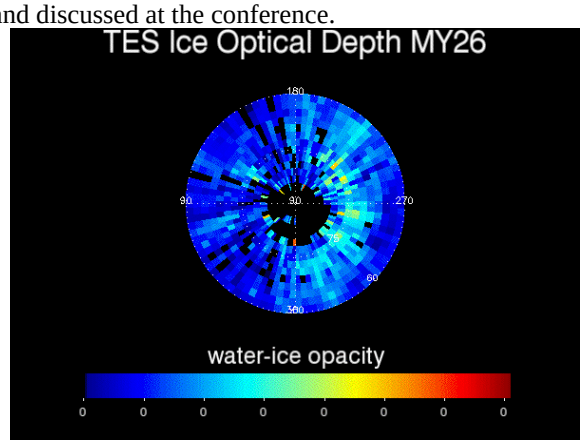

Figure 1. TES infrared (12-micron) water-ice optical depth map for MY26, L_s=95-110. The color scale bar ranges from 0-0.2.

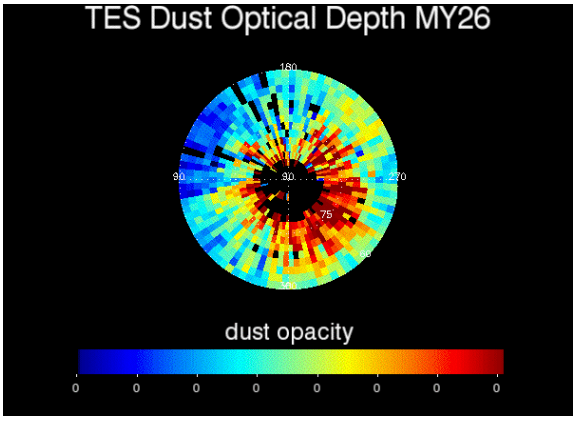

Figure 2. TES infrared (9-micron) dust optical depth map for MY26, L_s=95-110. The color scale bar ranges from 0-0.4.

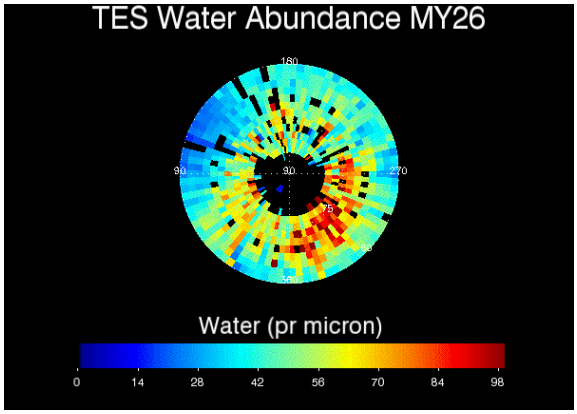

Figure 3. TES water vapor map for MY26, L_s=95-110. The color scale bar ranges from 0=100 pr microns.

Conclusions:

The water-ice cloud and dust optical depths and water vapor have been mapped in the north polar region during northern spring and summer for three Mars Years, beginning Ls=105 in MY24 (Mars Year definitions per Clancy et al., 2000), using the Mars Global Surveyor Thermal Emission Spectrometer (Tamppari *et al.*, 2005). The observations discussed here are consistent with past work on clouds and dust using other other techniques (e.g., Wang and Ingersoll; 2002, Smith, 2004; Cantor et al., 2001).

Specific conclusions are:

1) Longitudinal variability in the optical thickness of the NPH exists, both during springtime recession and late-summer onset. This variability varies interannually.

2) Each year, the breakdown of the seasonal NPH occurs about Ls=70 and the NPH reforms near about Ls=160-165. The end of the NPH did not vary interannually within the data set examined here, but the onset varied by about 5 degrees.

3) Late spring NPH recession water-ice clouds and mid-summer NPH onset water-ice clouds tend to be patchy in nature. In other words, they are confined near the northernmost extent of the data, but vary significantly in opacity as a function of longitude.

4) Water-ice cloud background opacity levels decrease to summertime low levels (typically <0.1) starting at Ls=80 in each year. The opacities begin to rise again at different times in different years: Ls=140 for MY 24, Ls=135 for MY 25, and Ls=110 for MY 26.

5) The background water-ice opacities appear to reach minimum values in the longitudinal region 0-90 W between Ls=105 and Ls= 125 in all years, though the onset and retreat of this feature was present earlier in MY 25 and continued later in both MY24 and 25. This observation is at the limit of the uncertainties in the data and cannot be confirmed.

6) The observations show many examples of water-ice clouds that are associated with elevated dust opacities as well as examples where water-ice clouds do not correlate with elevated dust opacities. Both types are seen at a variety of seasons and locations.

7) There is significant interannual variability in dust magnitude, but both MY 25 and 26 show peak dust (high magnitude over wide area) between Ls=75-100.

8) The longitudinal quadrant 0-90 W exhibits much higher dust opacities than other locations for many seasons in all years examined, but the details vary interannually. Both MY25 and 26 showed this region having the most dust between Ls=65-85.

9) There is evidence for stationary wavenumber 2 systems in the late spring in MY 26, characterized by elevated dust and water-ice in two opposite quadrants and reduced dust and water-ice in between.

10) Water vapor varies significantly interannually

11) Water vapor varies spatially within a season and different years behave differently.

12) Water vapor increases in some locations above 50 pr microns near L_s=75 and decreases below 50 pr microns again near L_s=130-125. In between times, there are many locations in which the column abundance is above 50 pr microns, even approaching 200 pr microns. This increase/decrease pattern is repeatable year to year.

Because these observations show the spatial and seasonal changes in atmospheric quantities over 3 Mars years, they will provide useful constraints for models of dynamics and water-ice cloud formation. In addition, the Phoenix Mars Scout Lander, scheduled for launch in August 2007, will land between 65-72 N in late May 2008. The mission will be 90 sols long, occurring between Ls=~76-125. Phoenix will have a stereo camera, with solar filters used for determining aerosol optical depth and water vapor abundance and an upward-looking, dual-wavelength, dual-detector lidar that will be able measure backscatter off atmospheric dust and water-ice. Understanding the likely behavior of water vapor, water-ice and dust in the atmosphere will enable better preparation of Phoenix observational sequences.

References in Alphabetical Order:

Briggs, G. A., and C. B. Leovy, *Bull. AMS*, **55**, 1975.
Boynton, W.V., et al., *Science* **297**, 2002.
Cantor, B., et al., *JGR* **106**(E10), 2001.
Christensen, P. R., et al., *JGR* **97**, 1992.
Clancy, R. T., et al. *JGR* **105**, 2000.
Christensen, P. R. et al., *JGR* **106**, 2001.
Farmer, C. B., et al, *Science* **194** (4271), 1976.
Feldman, W.C., et al., *Science* **297**, 2002.
Jakosky, B. M. and C. B. Farmer, *JGR* **87**, 1982

James PB, and Cantor BA, *Icarus* **154**(1), 2001.
James, P. B. et al., *Icarus* **109**, 1990.
Kieffer, H. H., *JGR* **84**, 1979.
Leovy et al., *Icarus* **17**, 1972.
Liu JJ, et al., *JGR* **108** (E8), 2003.
Martin, T. Z., and M. I. Richardson, *JGR* **98**(E6), 1993.
Pathak et al., submitted to *Icarus*, 2004.
Pearl et al., *JGR* **106**(E6), 2001
Smith, M.D., *Icarus* **167**, 2004.
Sprague, A. L. et al., *Icarus* **154**(1), (2001)
Tamppari, L. K., and D. S. Bass, *The 2nd Mars Polar Conf.*, 2003.
Tamppari et al., *JGR* **105**(E2), 2000.
Tamppari, L. K., et al., *JGR* **108**(E7), 2003.
Tamppari, L. K., *et al.*, submitted to *Plan. and Sp. Sci.*, 2005.
Wang HQ, Ingersoll AP, *JGR* **107**(E10), 2002.